

Decadal changes in the South Pacific western boundary current system revealed in observations and ocean state estimates

K. L. Hill,^{1,2} S. R. Rintoul,^{3,4,5} K. R. Ridgway,^{3,4} and P. R. Oke^{3,4}

Received 21 October 2009; revised 30 September 2010; accepted 12 October 2010; published 20 January 2011.

[1] Observations and ocean state estimates are used to investigate the nature and mechanism of decadal variability in the East Australian Current (EAC) system and South Pacific subtropical gyre. A 62 year record on the Tasmanian continental shelf shows decadal variations of temperature and salinity, as well as a long-term trend, which has been related to wind-driven variations in the poleward extension of the EAC. Repeat expendable bathythermograph lines spanning the last 15 years suggest that low-frequency variations in the transport of the EAC extension and Tasman Front are anticorrelated, but the time series are too short to draw firm conclusions. Here we use two ocean state estimates spanning the past 50 years to diagnose the physical mechanisms and spatial structure of the decadal variability of the South Pacific subtropical gyre. The observations and state estimates paint a consistent picture of the decadal variability of the gyre and EAC system. Strengthening of the basin-wide wind stress curl drives a southward expansion of the subtropical gyre. As the gyre shifts south, the EAC extension pathway is favored at the expense of the Tasman Front, resulting in the observed anticorrelation of the these two major currents. The results suggest that the subtropical gyre and western boundary current respond to decadal variability in basin-scale wind stress curl, consistent with Island Rule dynamics; that strong decadal variability of the South Pacific gyre complicates efforts to infer trends from short-term records; and that wind stress curl changes over the South Pacific basin drive changes in the EAC system that are likely to have implications for marine ecosystems and regional climate.

Citation: Hill, K. L., S. R. Rintoul, K. R. Ridgway, and P. R. Oke (2011), Decadal changes in the South Pacific western boundary current system revealed in observations and ocean state estimates, *J. Geophys. Res.*, 116, C01009, doi:10.1029/2009JC005926.

1. Introduction

[2] The East Australian Current (EAC) is the western boundary current of the wind-driven South Pacific subtropical gyre, and the mechanism by which warm salty water from low latitudes is transported southward, balancing the net equatorward Sverdrup transport of waters in the interior of the basin. The westward flow of the South Equatorial Current (SEC) forms the equatorward limb of the gyre. The SEC reaches the Australian coast between 15°S–22°S and bifurcates, with the southward flow feeding the EAC [Qu and Lindstrom, 2002]. Most of the EAC separates

from the coast at around 31–34°S to form the Tasman Front [Ridgway and Dunn, 2003; Mulhearn, 1987], which flows across the Tasman Sea and around the northern tip of New Zealand (NZ) to become the East Auckland Current. The remainder of the EAC (the EAC extension) continues south to the east coast of Tasmania, roughly following the shelf edge (see Figure 1).

[3] The pattern of wind stress curl determines the strength and spatial pattern of the gyre [Munk, 1950]. Hence variations in the basin-scale wind field will drive variability in the strength of the western boundary current. Understanding the dynamics of the relationship between boundary currents and remote wind forcing, and the timescales at which the ocean responds to changes in winds, is essential to explain the cause of observed variations in the western boundary currents at timescales from seasonal to multidecadal.

[4] The South Pacific gyre, and hence the EAC, exhibits a long-term strengthening trend related to a strengthening of the subtropical westerly winds in the South Pacific [Cai, 2006; Hill et al., 2008; Ridgway, 2007; Roemmich et al., 2007]. Hill et al. [2008] related decadal variability in the strength of the EAC, as reflected in temperature and salinity at the Maria Island time series station since 1944 to

¹CSIRO/UTAS Quantitative Marine Sciences Program, Marine and Atmospheric Research, CSIRO, Hobart, Tasmania, Australia.

²Now at Integrated Marine Observing System, University of Tasmania, Hobart, Tasmania, Australia.

³Centre for Australian Weather and Climate Research, CSIRO and Bureau of Meteorology, Hobart, Tasmania, Australia.

⁴CSIRO Wealth from Oceans Flagship, Hobart, Tasmania, Australia.

⁵Antarctic Climate and Ecosystems CRC, Hobart, Tasmania, Australia.

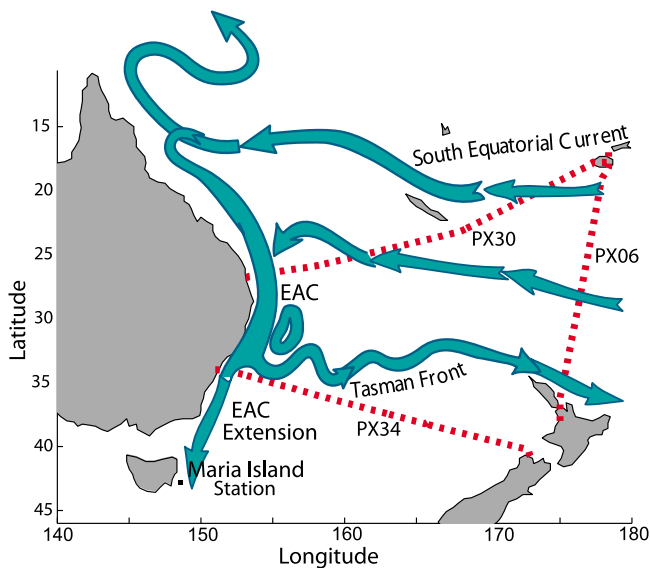


Figure 1. A schematic of Tasman Box XBT sections and the currents which cross them. The location of Maria Island coast station is also marked.

variability in the winds over the South Pacific using the Island Rule [Godfrey, 1989]. Temperature and salinity at Maria were correlated with changes in wind stress curl with a time lag of 3 years [Hill et al., 2008]. Roemmich et al. [2007] presented evidence of a spin-up of the South Pacific gyre between 1993 and 2004 from altimetric sea surface height (SSH), dynamic height and velocity data (calculated from hydrographic and float data). Roemmich et al. [2007] concluded that the subtropical gyre in the South Pacific has spun-up in response to increased Ekman pumping from increased wind stress curl. Roemmich et al. [2007] also noted a lag of 4–5 years between the peak in the wind forcing over the subtropical South Pacific, and the peak in the response of the ocean, in terms of the strength of the subtropical gyre circulation. Cai [2006] calculated the Sverdrup Island Rule solution for NCEP winds from the 1950s to the 1990s. Qiu and Chen [2006] identified a time lag of 2 years between changes in scatterometer-derived wind stress curl in the South Pacific and the ocean’s response in altimetric SSH.

[5] Observational studies of these long-term changes and variability are hampered by a dearth of long-term observations in the region. The 62 year record of temperature on the continental shelf off Maria Island, east of Tasmania is a notable exception. Hill et al. [2008] demonstrated a close relationship between changes in the wind stress curl, transport through the Tasman Sea and changes in temperature and salinity at Maria Island. However, the lack of corresponding observations over a broader region meant that it was not possible to relate the local variations to the flow of the EAC and the subtropical gyre as a whole. While a wealth of observations are available since the 1990s, the time series are too short to distinguish between trends and low-frequency variability. For instance, Roemmich et al. [2007] related observed changes in the gyre

during a 12 year period to the trend in the Southern Annular Mode, while Sasaki et al. [2008] relate gyre-scale changes in an 50 year eddy resolving ocean model hindcast to decadal ENSO variability via the Pacific South American mode. We examine the relationship between wind forcing and changes in the EAC and subtropical gyre.

[6] Here we combine information from 3 sources: a 62 year record from Maria Island, a 15 year time series of quarterly expendable bathythermograph (XBT) lines crossing the main currents in the southwest Pacific, and two ocean state estimates covering 50 years. We first compare 50 year ocean state estimates with the observations, and test whether the dynamical relationships (such as the time lag between wind forcing and the ocean’s response outlined above) seen in observations are found in the reanalyses. We then use the 50 year ocean state estimates to explore decadal variability in the South Pacific western boundary current system, building on previous studies of decadal changes and variability in the South Pacific gyre [Roemmich et al., 2007; Qiu and Chen, 2006; Cai et al., 2005; Cai, 2006; Sasaki et al., 2008]. In particular, we identify that the transport of the EAC extension and the Tasman Front are strongly anticorrelated, and this is caused by changes in wind stress curl changing the shape, and particularly the southern extent of the South Pacific gyre.

2. Data and Method

2.1. Observations

[7] The Maria Island coast station time series (42.5–42.6°S, 148.2–148.3°E) provides a 60 year time series of changes in temperature and salinity between the surface and 50 m that have been shown to be representative of large-scale circulation changes [Hill et al., 2008]. Details of the Maria Island coast station time series are presented by Ridgway [2007].

[8] Three XBT lines form a closed box in the South West Pacific, dubbed the Tasman Box [Roemmich et al., 2005]. These lines are PX06, Auckland to Fiji, PX30, Fiji to Brisbane and PX34, Sydney to Wellington (Figure 1). These lines cross the EAC, the southern core of the South Equatorial Current and the Tasman Front. These lines are occupied 4 times per year. XBT’s are dropped every 40 km in the open ocean, and every 15–20 km near shore. The Fiji to Brisbane and Sydney to Wellington lines have been running since 1991, and the Auckland to Fiji line has been running since 1986.

[9] We used a merged altimetry product from Archiving, Validation and Interpretation of Satellite Oceanographic Data (AVISO) [Ducet et al., 2000]. Data from Topex/Poseidon (T/P), Jason, ERS-1 and –2 and ENVISAT were combined in a $1/3^\circ \times 1/3^\circ$ Mercator grid, with one map every 7 days from November 1992 to December 2006. The AVISO fields are presented as anomaly fields relative to a 7 year mean from 1993 to 1998. However, for this study the fields were further adjusted to a background mean over the period 1992–2006.

2.2. Ocean State Estimates

2.2.1. German Estimating the Climate and Circulation of the Oceans

[10] German Estimating the Climate and Circulation of the Oceans (GECCO) is based on the 1 degree ECCO/MIT

adjoint ocean model, which is brought into consistency with satellite and in situ observations from 1952–2001 [Koehl and Stammer, 2007]. During the optimization, initial temperature and salinity conditions, as well as time-dependent surface fluxes of momentum, heat and freshwater are adjusted by an adjoint method in order to bring the model into agreement with observations. Background forcing consists of NCEP-1 wind stress, net heat and freshwater fluxes. This approach is mass and energy conserving.

[11] Comparison of GECCO with observations of the tropical Atlantic circulation suggests that GECCO produces the transports of the major currents well [Rabe *et al.*, 2008]. While the dynamically consistent assimilation scheme doesn't introduce artificial source or sink terms into the ocean, it was found that unresolved processes (in particular, due to coarse model resolution) may project onto forcing, so winds may not be realistic in all regions. While this appeared to be an effect on seasonal to interannual time-scales, Rabe *et al.* [2008] suggest long-term variability in wind stress forcing seems less perturbed in this way. The first 10 years of GECCO (1952–1962) were excluded from this study due to issues with long-term adjustment to the initial conditions or unresolved processes [Koehl and Stammer, 2007].

2.2.2. Simple Ocean Data Assimilation

[12] Simple Ocean Data Assimilation (SODA) version 2.0.2 is a 0.5° ocean state estimate covering the 44 year period between 1958 and 2001 forced by ERA-40 winds [Carton and Giese, 2006]. The model uses the Parallel Ocean Program (POP) model with an average resolution of 0.25° and 0.4° in the zonal and meridional directions and 40 vertical levels, which was then remapped onto a 0.5° by 0.5° grid for distribution and archival.

[13] SODA employs a sequential data assimilation scheme that uses fields from the numerical model as a background field at the update time. At each assimilation step, an optimal interpolation technique is used to compute an analysis by combining the background field with an array of observations. The model is initialized with the analysis and integrated forward in time until the next assimilation step. The adjustments of the model field introduced by the assimilation procedure do not generally conserve mass or energy.

[14] Steric sea level rise was assessed by comparing SODA version 1.2 with 20 tide gauge station sea level records from around the world (selected for data length; coverage of ocean basins and latitudes; and sites exposed to the open ocean or on narrow continental shelves) on subseasonal timescales [Carton *et al.*, 2005]. It was found that a positive relationship was found at all gauge stations, with an average correlation of $r = 0.7$. This represents a substantial improvement on previous versions of the SODA reanalysis. Carton *et al.* [2005] also compared the SODA dynamic height with altimeter sea level, and found very good spatial agreement in the linear trends. This is promising considering that altimeter data is excluded from the reanalysis.

2.3. Calculations and Analysis

[15] Times series of geostrophic transport across each Tasman Box section (relative to 2000 m) were calculated using a combined altimeter/XBT technique [Ridgway *et al.*, 2008]. Subsurface T and S structure is inferred from surface

sea level anomaly using an empirical model developed from historical observations. The transport is then computed directly from the T and S data. XBT data are used to both provide accurate mean fields along each section and to validate the results from altimetry. Estimates of net transport between Sydney and Wellington from the altimeter method agree closely with independent measurements from CTD sections [Ridgway *et al.*, 2008].

[16] Full depth total transports across the Tasman Box lines (Figure 1) are computed using fields from GECCO and SODA. For SODA, calculations require some interpolation and approximation to accommodate the numerical B grid used and the limitations due to the storage of averaged fields. For GECCO, the the model uses a C grid, which means that interpolation is not needed to calculate transports.

[17] Wind stress curl was calculated from ERA-40 winds for comparison with SODA results, and NCEP winds (as well as NCEP winds optimized by GECCO) for GECCO. The quality of these products has been discussed in the literature, and a number of differences were highlighted [Bromwich and Fogt, 2004]. However, low-frequency variability in the basin-wide wind stress curl is similar in ERA-40 and NCEP, as well as the GECCO-optimized NCEP winds. Wind stress curl in the region $180\text{--}280^\circ\text{E}$, $20\text{--}50^\circ\text{S}$ was selected for comparisons with the model temperature and salinity at the location of Maria and transport through the Tasman Sea following analysis of the relationship of the spatial cross correlation of South Pacific winds stress curl with Maria temperature by Hill *et al.* [2008].

[18] The Tasman front transport calculated from the reanalyses was defined as the maximum cumulative eastward transport across the southern section of the Auckland to Fiji line (calculated at each depth level). The northern limit of the integration was identified from the mean cross-section velocity fields. We define this as 28°S for SODA, and 27°S for GECCO. A different cut off latitude was used for each reanalysis product, as differing resolution affects the structure of the circulation. For instance, in GECCO, features such as the Tasman Front are smoother and broader due to the reduced resolution. As the Sydney to Wellington section crosses close to the point where a portion of the EAC separates from the coast to form the Tasman Front, the transport calculations could be contaminated by eddies if the same method was employed there. Therefore, the EAC extension transport was defined as the net southward transport through the Tasman Sea, across the Sydney to Wellington line. All time series were low pass filtered with a 5 year running mean and cross correlations were carried out on filtered data with a linear trend removed.

3. Results

3.1. Low-Frequency Variability of the South Pacific Subtropical Gyre

[19] These reanalyses provide the best estimate of the three-dimensional ocean state over the past 50 years. We use both observations and reanalysis to explore the nature of the low-frequency variability of the gyre, and also test how well the reanalyses can simulate observed variability and dynamical relationships. To do this, we compare the reanalyses with the available observations to see to what

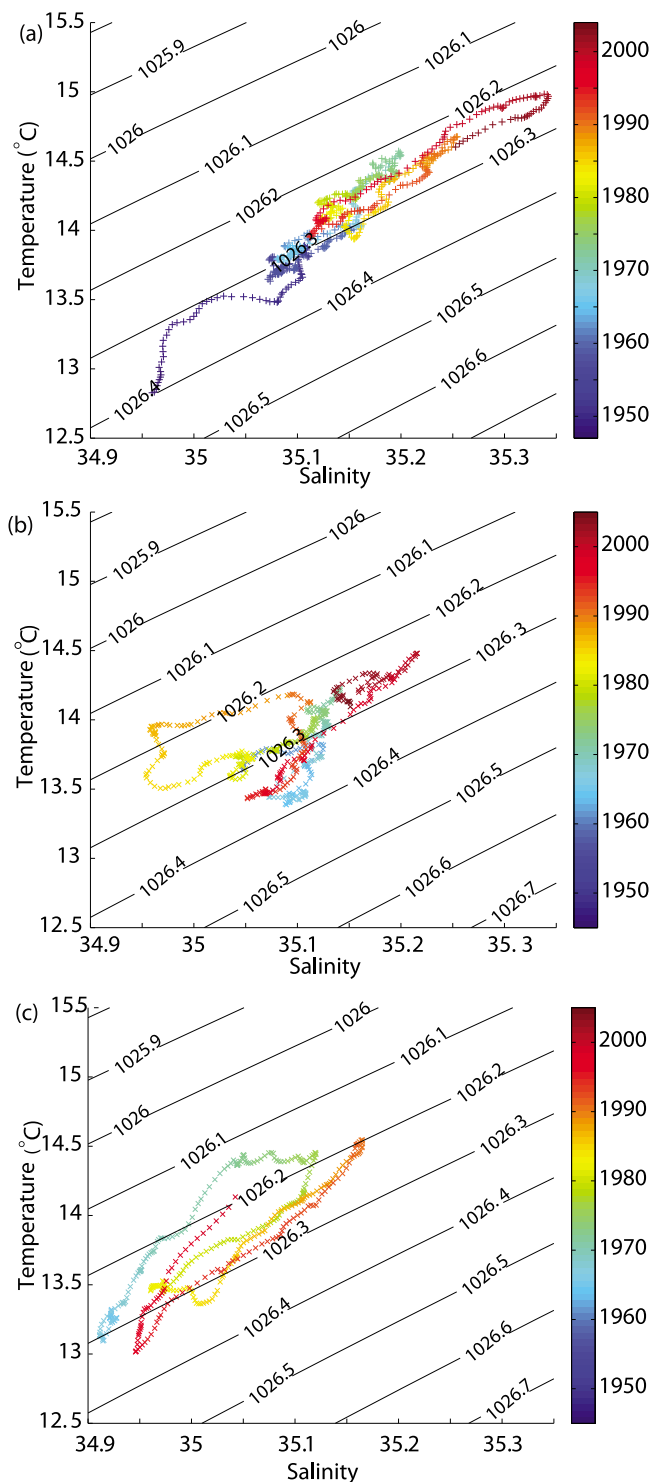


Figure 2. Surface temperature–salinity plots for (a) Maria, (b) SODA at Maria, and (c) GECCO at Maria. The color bar indicates the year of the data point.

extent they agree in terms of: water mass properties and variability; the relationship between water mass variability, boundary current transport and forcing; and model vertical structure.

3.1.1. Temperature and Salinity at Maria Island Coastal Station

[20] The observed temperature–salinity (T–S) diagram at Maria Island shows a very clear relationship between changes in temperature and salinity, varying from cooler fresher waters, to warmer saltier waters (Figure 2a). This suggests that these changes represent an advected signal, which is related to variations in the strength of the EAC, rather than changes in atmospheric heating, the evaporation/precipitation balance, or in river outflow which would cause one to change without the other [Hill *et al.*, 2008]. Both SODA and GECCO show a similar relationship, with properties varying from cold and fresh to warm and salty centered on the 1026.3 kg/m³ density contour (Figures 2b and 2c). SODA is less able to preserve this T–S relationship in the 1980s, when a large drop in salinity (from 35.1 to 34.95 psu) is seen without an associated drop in temperature. Both SODA and GECCO are cooler and fresher than the observations. The slope of the T–S relationship in GECCO and SODA is similar to that found in Maria (+1°C change in temperature = +0.15 psu change in salinity); and this slope is consistent with a north–south translation of the meridional temperature and salinity gradients along the east coast of Australia [Hill *et al.*, 2008].

3.1.2. The Relationship Between Water Mass Properties, Wind Forcing, and Volume Transport

[21] Hill *et al.* [2008] demonstrated that the strength of the EAC is closely related to the magnitude of wind stress curl in the South Pacific on decadal timescales, with a time lag of 3 years. We compare the relationship between model temperature and salinity at the location of Maria Island coast station with South Pacific wind stress curl, and net transport through the Tasman Sea (Figure 3). Both models show decadal variability in temperature and salinity at Maria, South Pacific wind stress curl and transport through the Tasman Sea at a similar phase and frequency; corroborating the findings of Hill *et al.* [2008] that observed temperature and salinity at Maria could be related to transport through the Tasman Sea using the Island Rule.

[22] The precise relationship between properties at Maria, wind stress curl in the South Pacific and transport through the Tasman Sea differs slightly between models. Lagged cross correlation between SST at the location of Maria, and volume transport through the Tasman Sea (at 43°S) for SODA peak at only $r = 0.4$ when SST lags transport by 24 months; while the time lag is consistent with observations [Hill *et al.*, 2008; Qiu and Chen, 2006] the low correlation value suggests a poor correspondence in the model between variations in the volume transport through the Tasman Sea, and variations in SST and salinity at Maria. Changes in SODA volume transport through the Tasman Sea and changes in the wind stress curl in the South Pacific (20–50°S, 180–280°E) show correlations (r) of 0.68 at zero lag. The net volume transport is close to observed, with values of 6–9 Sv compared to 9.4 Sv [Ridgway and Godfrey, 1994]. However, while the winds, transport and T/S properties at Maria seem to be comparable to observations since the mid 1980s, the relationship seems to be less consistent prior to the mid-1980s, or presatellite era.

[23] The GECCO South Pacific wind stress curl and transports through the Tasman Sea (Figures 3c and 3d) show

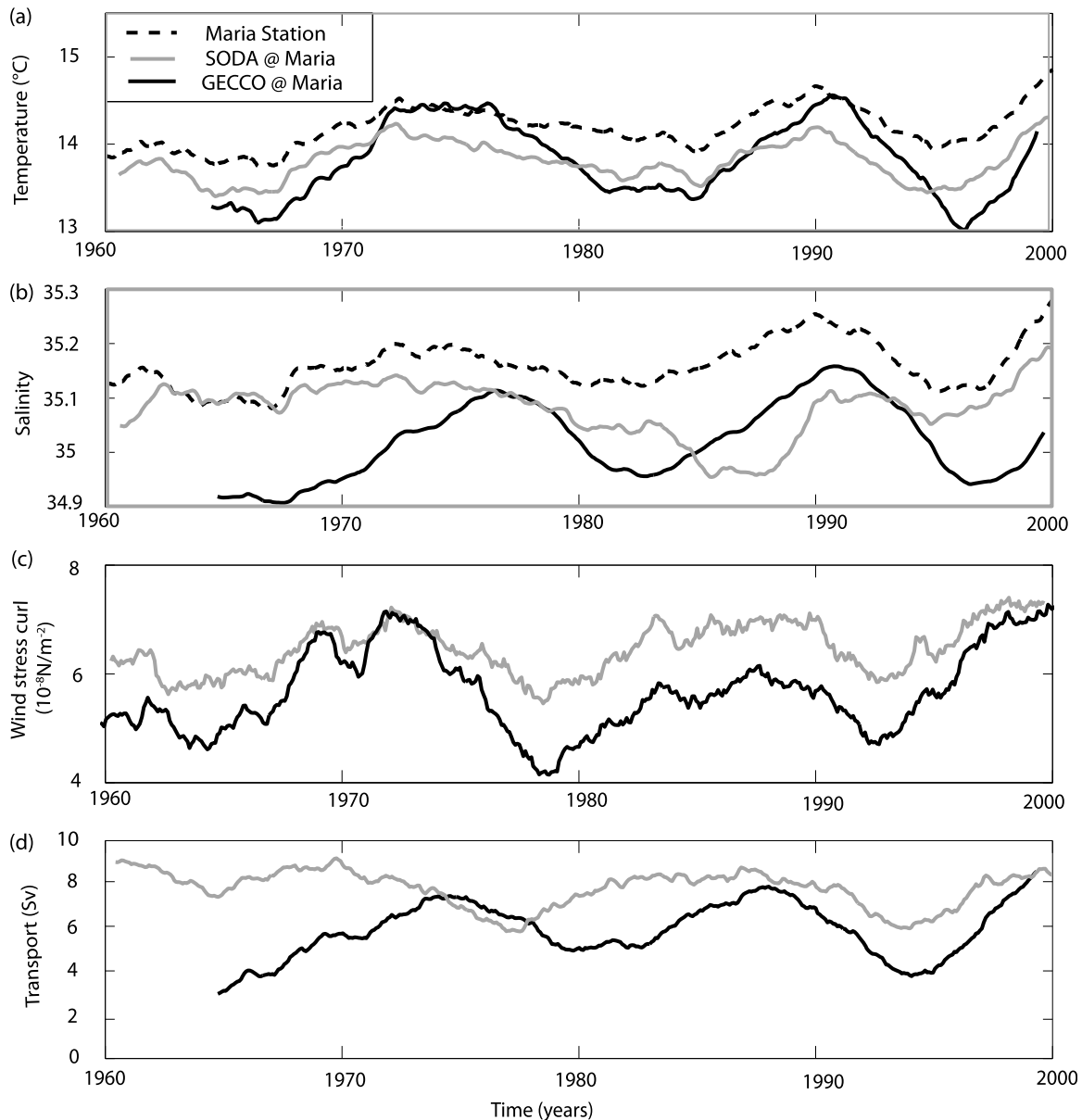


Figure 3. Time series of (a) SST at Maria (observed) and at the location of Maria in SODA and GECCO, (b) sea surface salinity at Maria (observed) and at the location of Maria in SODA and GECCO, (c) ERA-40 and GECCO-optimized NCEP South Pacific regional mean wind stress curl (180–280°E, 20–50°S), and (d) SODA and GECCO net southward transport through the Tasman Sea.

similar frequency and timing of variability to the GECCO temperature time series, with a strong decadal variability signal. Changes in wind stress curl lead changes in transport by 18 months ($r = 0.65$), and changes in temperature lag changes in wind stress curl by 36 months ($r = 0.65$). Even in this model with more complete physics, changes in transport still lead the temperature response by 20 months ($r = 0.8$). The magnitude of transport through the Tasman Sea is consistently low compared to observations, with a range of 3–8 Sv compared to an observed mean of 9.4 Sv [Ridgway and Godfrey, 1994]. The robustness of the relationship between temperature and salinity at the location of Maria, winds in the South Pacific and transport through the Tasman

Sea, suggests that the dynamical response of the GECCO model to changes in winds is consistent with observations [Hill *et al.*, 2008].

3.1.3. Vertical and Horizontal Ocean Structure

[24] In order to simulate the ocean's response to wind forcing, two aspects of the model fields need to be realistic: the vertical structure, to ensure realistic Rossby wave propagation and communication of changes in forcing to the western boundary; and the position and magnitude of regional ocean currents. Although the Tasman Box XBT lines only span a 15 year period, they provide the only long-term measurements of subsurface ocean variability in the region. Mean temperature sections from XBTs, SODA and GECCO for the

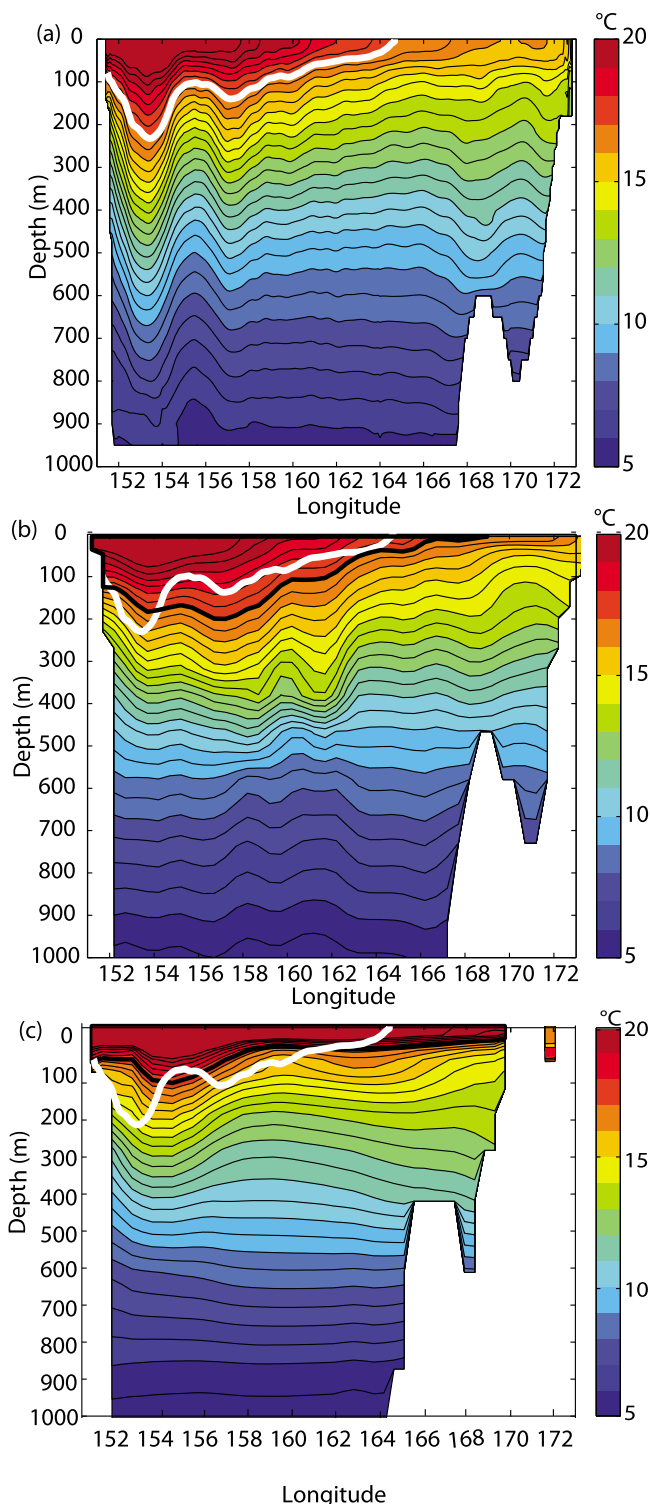


Figure 4. Temperature along PX34 from (a) XBT data, (b) SODA, and (c) GECCO for overlapping years (1993–2001). Models are sampled during months when the XBT section was occupied. Thick black contour indicates 17°C isotherm for models, and white lines indicate 17°C isotherm from XBT data for comparison.

period 1993–2001 (Figure 4) all show the warm core of the EAC in the western portion of the section. The 17°C isotherm from the XBT data is plotted on each section for comparison. The model representation of the mesoscale structure along this section is related to the model resolution. For instance, the zonal extent of the 17°C isotherm at the surface increases with decreasing spatial resolution. The XBT data and SODA show a secondary warm core to the east of the main EAC, reflecting a semi permanent meander of the Tasman Front [Ridgway and Dunn, 2003]. Below the surface, the sloping isotherms of the EAC penetrate to at least 900m in the XBT section (the limit of the XBT observations); SODA and GECCO's isotherms flatten out at around 600m. In addition, GECCO does not reproduce the complex frontal structures across the Tasman Sea, which are likely associated with meanders in the Tasman Front.

[25] We next examine the inflow to the western boundary of the South Pacific in observations and the reanalyses. The observations and models show similar transports across Sydney to Wellington (PX34) in terms of both magnitude and frequency/phase of decadal variability (not shown). However, volume transports across the Auckland to Fiji line (PX06) and the Brisbane to Fiji line (PX30) are very different in observations and state estimates. Mean eastward cumulative transport is calculated for XBT/altimeter, SODA and GECCO from south–north along the Auckland to Fiji line, and then a section north of Fiji along 180°E for SODA and GECCO (Figure 5). Starting in the south, the Tasman Front is stronger and wider in GECCO and SODA than observed. The eastward flow in the Tasman Front is balanced by the westward flowing SEC component to the south of Fiji, which is stronger in SODA (-22 Sv) than in GECCO (-17 Sv). SODA and XBT/altimeter therefore show a net inflow into the Tasman Sea south of Fiji of around 10 Sv , while GECCO shows a smaller net inflow of 2 Sv . A larger fraction of the total SEC transport occurs north of Fiji in GECCO than in SODA, although in both models the bulk of the SEC is found north of Fiji. Changes in the net transport across the Auckland to Fiji line can be caused by changes in the strength of the Tasman Front, changes in the strength of the SEC, or changes in the partitioning of the SEC flow north and south of Fiji.

[26] To summarize, both models exhibit similar decadal variability to that seen in observations. GECCO better reproduces the dynamical relationships and time lags seen in observations, such as the close relationship between variations in temperature and salinity at Maria, and the time lag between changes in South Pacific winds and the transport response of the EAC. SODA provides a more accurate ocean state estimate at any given time, but it is less able to recreate the dynamical relationships seen in observations, particularly prior to the satellite era. Both ocean state estimates reproduce the vertical structure and major current systems of the western South Pacific, although with some smoothing as expected given the model resolution. While significant differences exist between the two state estimates reflecting differences in forcing data used, assimilation approach and resolution, each reproduces the observed ocean structure with sufficient fidelity to be useful as a tool to explore the nature and causes of low-frequency variability in the South Pacific subtropical gyre.

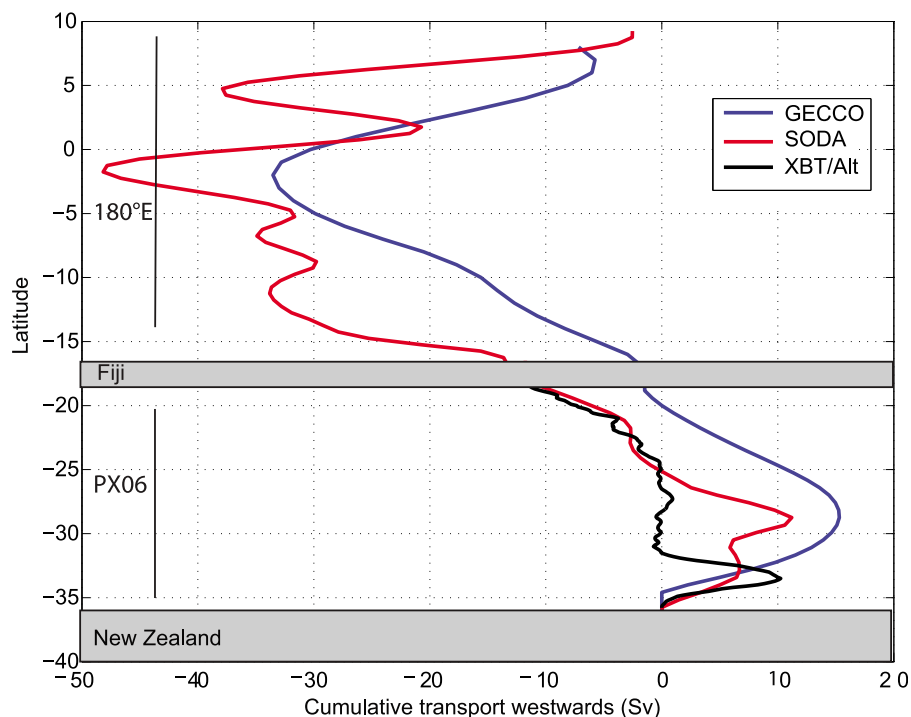


Figure 5. Cumulative eastward transport across PX06 and north of PX06 across 180°E for GECCO, SODA, and combined XBT/altimeter 1993–2001.

3.2. Wind-Driven Decadal Variability of the South Pacific Gyre

3.2.1. Outflow Pathways From the Tasman Sea

[27] Water carried south by the EAC exits the Tasman Sea by one of two pathways: the EAC extension or the Tasman Front (Figure 1). Transports estimated from the XBT sections suggest the two branches are of roughly equal magnitude and strongly anticorrelated, at least for the short period spanned by the observations (Figure 6a). In the state estimates, the Tasman Front is consistently larger than the EAC extension, particularly in the lower-resolution GECCO model (Figures 6b and 6c). Transports estimated from a 1/10° state estimate (the BlueLink Reanalysis [Schiller *et al.*, 2008]) show a weaker Tasman Front and stronger EAC extension, more consistent with the XBT observations [Hill, 2009]. These results suggest that higher-resolution models are more successful in capturing the dynamics of the EAC separation and the observed partitioning into the two outflow pathways.

[28] However, despite the differences in the mean transport of the EAC extension and Tasman Front, the transport of the two branches is anticorrelated in the state estimates, as observed. This is more clearly seen by detrending the two time series (Figures 8a and 8b). Both models show an inverse relationship between the strength of the EAC extension and the Tasman Front, with correlations of $r = -0.62$ (SODA) and -0.8 (GECCO) at zero lag. (The relationship does not hold prior to about 1980 in SODA, when, as discussed above, SODA tends to diverge from the observations.)

[29] These results suggest that the outflow oscillates between the EAC extension and Tasman Front pathways on

decadal timescales. Both GECCO and SODA agree with the XBT/altimeter during the short period of overlap between 1995 and 2000, with all time series showing a transition from a minimum in EAC extension and a maximum in the Tasman Front transport in 1995, to a maximum in the EAC and a minimum in the Tasman Front in 2000. The fact that both state estimates consistently produce the anticorrelation between the EAC extension and the Tasman Front, despite the differences highlighted above, suggests that this is a robust result.

[30] The decadal variations in the strength of the EAC extension and Tasman Front have a consistent relationship with low-frequency variability of the wind stress curl over the South Pacific. Figures 8c and 8d shows a longitude-time plot of zonal mean wind stress curl for the two models. The region of maximum wind stress curl sits between 40 and 50°S and 45 and 50°S for SODA and GECCO, respectively. In both models, the strength of the wind stress curl varies on decadal timescales, with maxima centered on 1960 (in SODA), 1972, 1988, and 2000. These can each be associated with maxima in the transport of the EAC extension, and minima in Tasman Front transport, a few years later in both reanalyses (Figures 8a and 8b). Similarly, a few years after a minimum in the wind stress curl, Tasman Front transport peaks and EAC extension transport reaches a minimum.

3.2.2. Island Rule

[31] Hill *et al.* [2008] showed that the net transport through the Tasman Sea estimated from Godfrey's [1989] Island Rule varied on decadal timescales and was coherent with variations in temperature and salinity at Maria Island. The Sverdrup dynamics underlying the Island Rule can

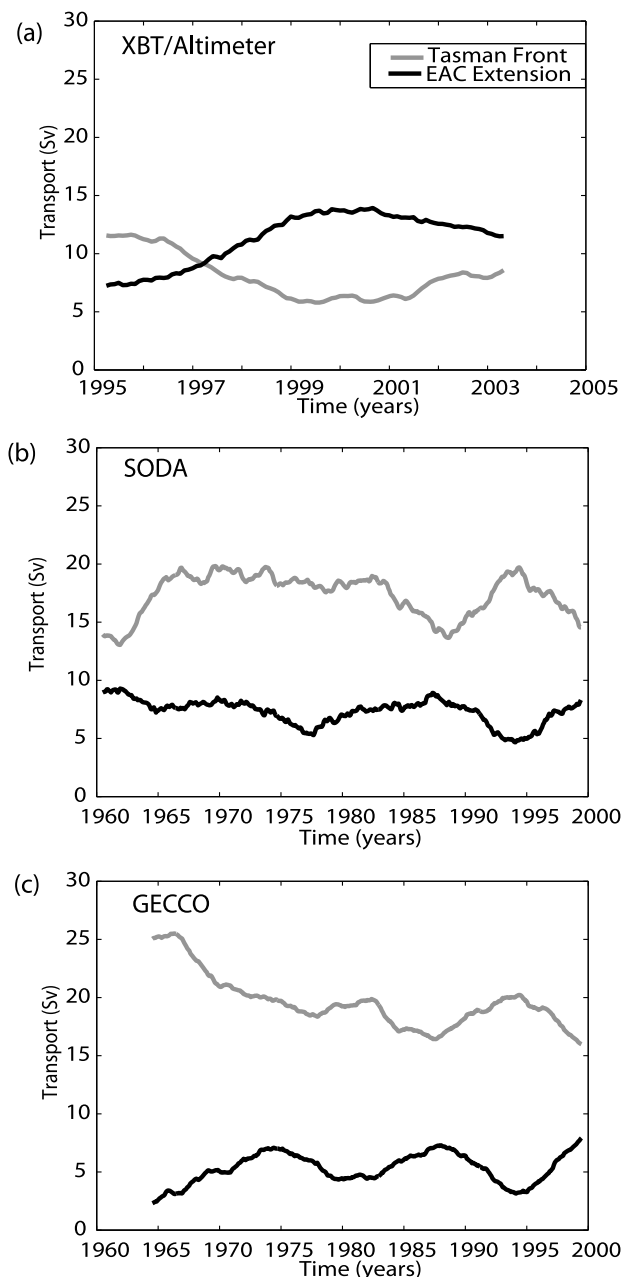


Figure 6. Transports for the Tasman Front and EAC extension calculated using a combined (a) altimeter/XBT method, (b) SODA reanalysis, and (c) GECCO reanalysis. Note that the x axis for Figure 6a differs from Figures 6b and 6c.

account for much of the low-frequency variability of the flow through the Tasman Sea in the state estimates as well. Figure 7 compares the net transport through the Tasman Sea estimated from the Island Rule and from the two state estimates. All four curves show similar quasi-decadal variability. The Island Rule and SODA transports are roughly in phase, while the GECCO transports lag the Island Rule values by 1–2 years. As noted in the discussion of Figure 3, the lag seen in GECCO between wind changes and the transport/temperature response on the western boundary is more consistent with observations.

[32] The Island Rule transports are significantly larger than found in SODA and GECCO. The Island Rule transport increase between 1995 and 2000 is also larger than observed in the XBT sections, by about a factor of two (compare Figures 6 and 7). The state estimates, on the other hand, tend to underestimate the transport through the Tasman Sea, as discussed above. The difference between the Island Rule and the reanalyses therefore likely reflects an overestimate of the EAC extension by the Island Rule approximation and an underestimate by the state estimates.

[33] The consistency between the simple Island Rule estimates and the modeled transport further supports the conclusion that low-frequency variability in basin-scale winds drives changes in the partitioning of the outflow from the Tasman Sea between the EAC extension and the Tasman Front.

3.2.3. Decadal Variations in the South Pacific Gyre

[34] Variations in the strength of the EAC extension and Tasman Front are linked to basin-scale changes in the South Pacific gyre. To illustrate this, we compare the depth-integrated stream function in years of maximum and minimum transport in the two pathways (Figure 9). In 1994, when the Tasman Front is stronger (see Figure 8), the South Pacific circulation has a single gyre structure in both SODA and GECCO, with the bulk of the gyre recirculating to the north of New Zealand. Tighter streamlines are seen across the Tasman Sea and to the north of New Zealand, with the Tasman Front carrying 15 Sv (SODA) and 20 Sv (GECCO) to the east.

[35] In 1988 when the EAC extension is favored (see Figure 8), transport through the Tasman Sea increases by 5 Sv. In SODA, the gyre extends further south and east, with stronger circulation in the latitude range of New Zealand. In GECCO, the South Pacific circulation has a double gyre structure, with a second gyre to the east of New Zealand between 35 and 50°S and extending east to 120°W. In both models, the subtropical gyre has expanded southward to enclose New Zealand. The Tasman Front transport is reduced to 10 Sv (SODA) and 15 Sv (GECCO). Similar changes in the strength and southern extent of the gyre are found for other realizations of the EAC extension and Tasman Front favoured state(not shown), which suggests that the two states reflect robust gyre-scale changes throughout the 50 years of both SODA and GECCO.

[36] In both GECCO and SODA, a stronger wind stress curl maximum favors a broader gyre structure partially encircling New Zealand (Figure 9) and stronger transport through the Tasman Sea. A weaker wind stress curl maximum appears to favor a state where New Zealand sits outside of the gyre, with the bulk of the transport recirculating north of New Zealand in the Tasman Front.

4. Discussion and Conclusions

[37] Previous studies have documented a spin-up of the South Pacific gyre in the 1990s from in situ observations and satellite altimeter data [Qiu and Chen, 2006; Roemmich et al., 2007; Sutton et al., 2005]. Roemmich et al. [2007] related the spin-up of the gyre to an increase in wind stress associated with the positive trend in the Southern Annular Mode (SAM). The much longer record obtained here from the ocean state estimates supports the conclusion

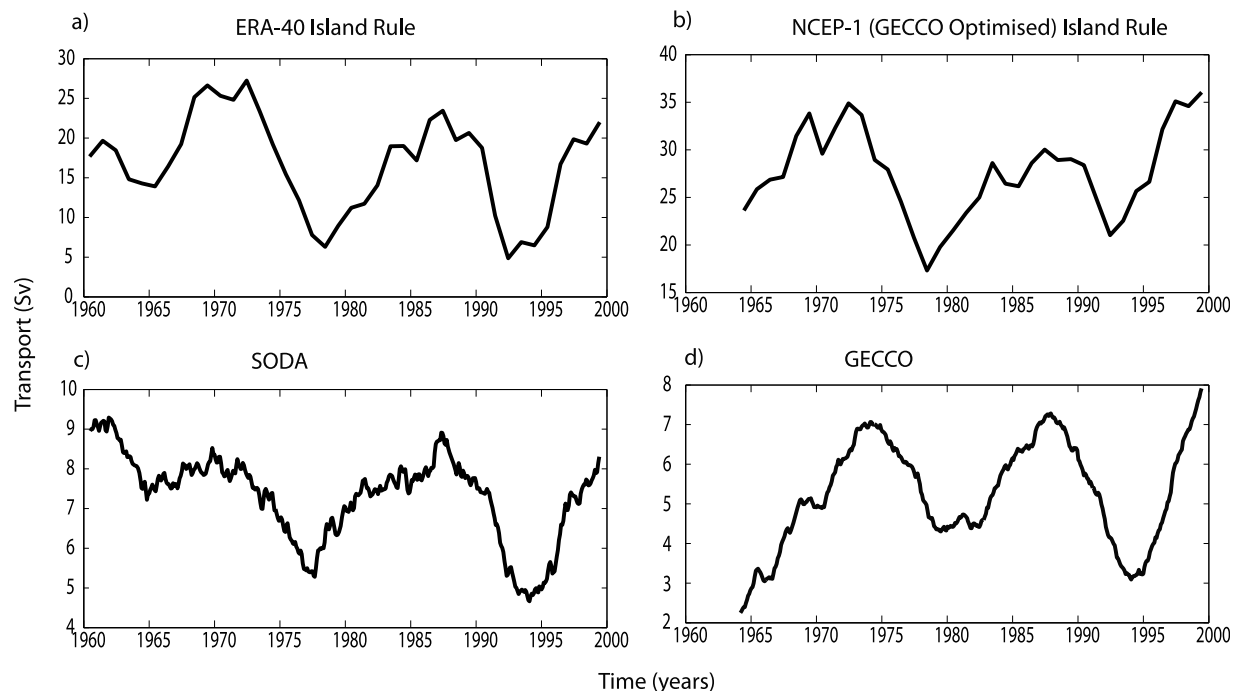


Figure 7. Island Rule transport through the Tasman Sea for (a) ERA-40 (winds used to force SODA) and (b) GECCO-optimized NCEP-1 compared with model transports for (c) SODA and (d) GECCO.

reached from analysis of the Maria Island time series that the spin-up of the gyre during the 1990s was associated with a strong quasi-decadal oscillation in the gyre, as well as a long-term trend. *Cai* [2006] also concluded from an Island Rule calculation that the South Pacific gyre had increased and shifted to the south over the last 50 years in response to strengthened westerly winds associated with the Southern Annular Mode.

[38] *Sasaki et al.* [2008] also investigated the variability of the South Pacific gyre. Like the prior studies, they concluded that changes in the gyre were associated with decadal variability in wind stress curl, but they attributed the wind changes to decadal variations in ENSO rather than the SAM. Wind stress curl east of New Zealand was highly correlated with the first empirical orthogonal function (EOF) of sea level variability in the OFES model. Wind stress variability in this region was linked to the Pacific South American mode, the atmospheric teleconnection linking tropical Pacific variability to higher latitudes [*Garreaud and Battisti*, 1999; *Mo*, 2000]. The region east of New Zealand makes the dominant contribution to decadal variability in zonal mean wind stress curl in the forcing fields used to drive the models examined here (Figures 8c and 8d). The results of *Sasaki et al.* [2008] suggest that the decadal oscillation between the EAC extension and Tasman Front pathways, shown here to be driven by wind forcing east of New Zealand, may be linked to decadal ENSO. However, the relative contribution of ENSO and SAM to low-frequency variability in wind stress curl between 40 and 50°S, and hence the variability of the South Pacific gyre, has not yet been determined.

[39] *Sasaki et al.* [2008] also noted that positive sea level anomalies (SLAs) in the South Pacific coincided with

weaker eastward currents in the Tasman Front and a decrease in eddy activity north of the front. Our study takes this relationship a step further by showing that wind stress curl variability over the South Pacific drives gyre-scale changes in circulation. The two studies support the conclusion that enhanced wind stress curl east of New Zealand results in a southward expansion of the subtropical gyre, a stronger EAC extension and a weaker Tasman Front.

[40] Transport estimates based on the Island Rule reproduce the decadal oscillation between the two outflow pathways from the Tasman Sea. This suggests that the gyre response to low-frequency variability in wind stress curl can be largely explained by the simple Sverdrup dynamics that underpin the Island Rule. The details of the dynamical response, however, are not yet entirely clear. *Qiu and Chen* [2006] and *Sasaki et al.* [2008] conclude that a linear model based on propagation of long baroclinic Rossby waves can reproduce a large part of the observed sea level variability in the South Pacific. *Sasaki et al.* [2008] also highlighted the role of Kelvin waves propagating around New Zealand and spawning Rossby waves in the Tasman Sea. However, in both cases, the linear models were not able to reproduce the observed variability in sea level in the southern and western Tasman Sea. The rapid response of the boundary current system to wind stress curl changes, observed here and by *Hill et al.* [2008], is also difficult to explain with only baroclinic waves. The details of the dynamical response are difficult to unravel from the ocean state estimates, in which the ocean variability reflects the response to a variety of forcing mechanisms and timescales. In a follow-up study to this work, we are using an ocean general circulation model forced with idealized wind perturbations to elucidate the role

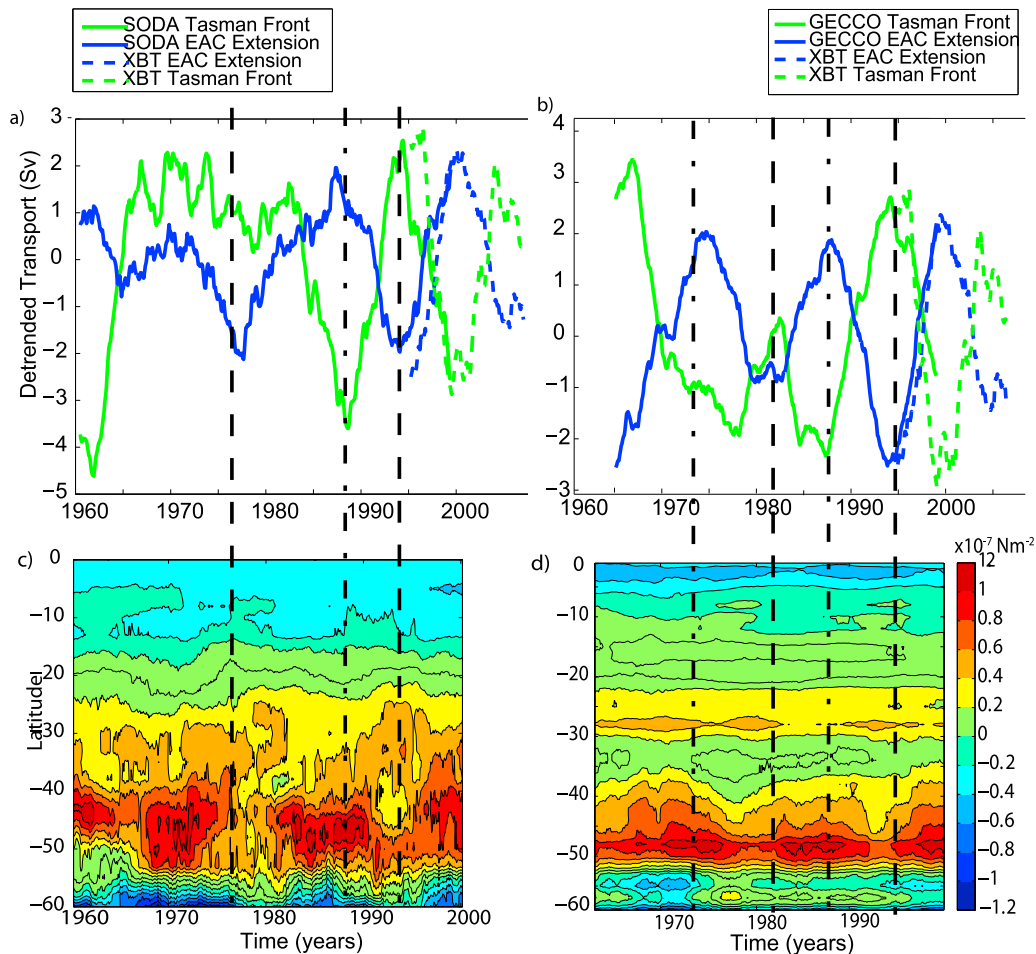


Figure 8. EAC extension and Tasman Front transport (Sv) in (a) SODA and (b) GECCO (linear trend removed) and South Pacific zonal mean wind stress curl (180–280°E) for (c) SODA (ERA-40) and (d) GECCO (GECCO-optimized NCEP-1).

of baroclinic and barotropic waves in the transient response of the gyre to changes in wind stress curl.

[41] Progress in understanding of the low-frequency variability of the ocean circulation has been slowed by the lack of long-term observations. Very few ocean time series are of sufficient duration to resolve decadal and multidecadal variability. The long time series that do exist are often limited to a particular location (e.g., the 60 year record from Maria Island). In this study we have attempted to overcome this hurdle by use of ocean state estimates spanning the last 50 years. Global ocean state estimates have only become available in recent years and their utility for studies of low-frequency variability in the ocean has not yet been demonstrated in many studies. Comparison of the two state estimates with each other, and with the long-term data sets from Maria Island and the Tasman Box XBT lines, suggests that, while substantial differences exist between them, the reanalyses have sufficient skill to be useful tools for the study of ocean variability. In particular, the fact that the two state estimates, despite their differences, provide a consistent picture of the relationship between changes in wind forcing, changes in the strength and extent of the gyre, and

the inverse relationship between the EAC extension and Tasman Front gives confidence that the results are robust.

[42] The decadal variability of the gyre and boundary currents discussed here has implications for ecosystem management. In recent years, the strengthening of the EAC extension has been linked to a southward range expansion of a number of marine species, across a range of taxa, down the east coast of Australia [Lyne *et al.*, 2005; Ling *et al.*, 2008; Ling, 2008; Last *et al.*, 2010]. Climate change models suggest the Tasman Sea is expected to continue to warm in the future, in part because of strengthening of the EAC. The increased transport facilitates the southward advection of larvae, and the warmer water temperatures permit the southward expansion of species close to the lower limit of their temperature tolerance. The decadal switching between an EAC extension-favored and Tasman Front-favored state is likely to have implications for larval transport in the Tasman Sea region and for the interpretation of trends based on short ecological time series. Strategies for management of marine resources in southeastern Australia will need to take into account the response of regional oceanographic conditions to climate variability in the context of climate change.

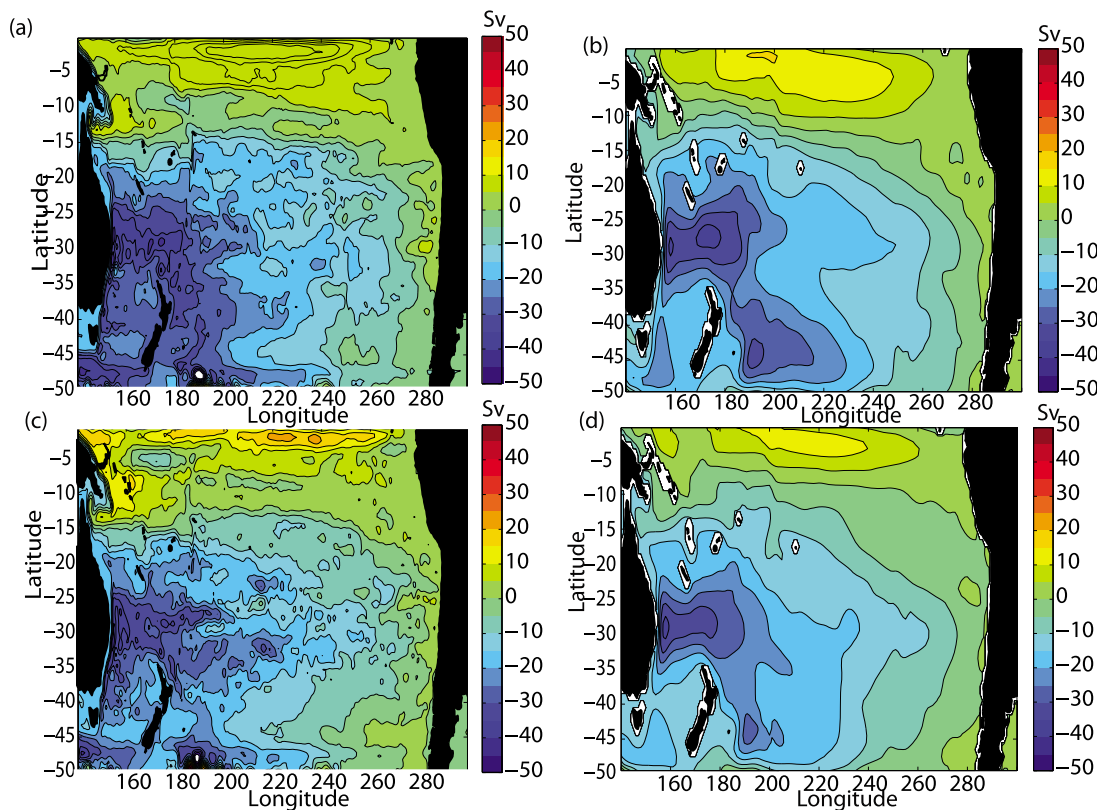


Figure 9. SODA (Figures 9a and 9c) and GECCO (Figures 9b and 9d) annual mean stream functions for (a and b) 1988 (stronger EAC extension, weaker Tasman Front) and (c and d) 1994 (weaker EAC extension, stronger Tasman Front). Contours every 5 Sv.

[43] **Acknowledgments.** The authors would like to thank Bernadette Sloyan, George Cresswell, and two anonymous reviewers for their thoughtful comments and Ben Geise and Armin Koehl for their help and patience in data matters. This work was conducted as part of the Quantitative Marine Sciences Ph.D. Program, a joint initiative between the University of Tasmania and CSIRO. This study was supported in part by the Department of Climate Change and Energy Efficiency through the Australian Climate Change Science Program and the Australian Government Cooperative Research Centre (CRC) program through the Antarctic Climate and Ecosystems CRC.

References

- Bromwich, D. L., and R. L. Fogt (2004), Strong trends in the skill of the ERA-40 and NCEP-NCAR reanalyses in the high and midlatitudes of the Southern Hemisphere, *J. Clim.*, *17*, 4603–4619.
- Cai, W. (2006), Antarctic ozone depletion causes an intensification of the Southern Ocean super-gyre circulation, *Geophys. Res. Lett.*, *33*, L03712, doi:10.1029/2005GL024911.
- Cai, W., G. Shi, T. Cowan, D. Bi, and J. Ribbe (2005), The response of the Southern Annular Mode, the East Australian Current, and the southern mid-latitude ocean circulation to global warming, *Geophys. Res. Lett.*, *32*, L23706, doi:10.1029/2005GL024701.
- Carton, J., B. Giese, and S. Grodsky (2005), Sea level rise and the warming of the oceans in the Simple Ocean Data Assimilation (SODA) reanalysis, *J. Geophys. Res.*, *110*, C09006, doi:10.1029/2004JC002817.
- Carton, J. A., and B. S. Giese (2006), A reanalysis of ocean climate using Simple Ocean Data Assimilation SODA, *Mon. Weather Rev.*, *136*(8), 2999–3017.
- Ducet, N., P. Y. Le Traon, and G. Reverdin (2000), Global high-resolution mapping of ocean circulation from TOPEX/POSEIDON and ERS-1 and -2, *J. Geophys. Res.*, *105*, 19,477–19,498.
- Garreaud, R. D., and D. S. Battisti (1999), Interannual (ENSO) and interdecadal (ENSO-like) variability in the Southern Hemisphere tropospheric circulation, *J. Clim.*, *12*, 2113–2123.
- Godfrey, J. S. (1989), A Sverdrup model of the depth-integrated flow for the world ocean allowing for island circulations, *Geophys. Astrophys. Fluid Dyn.*, *45*, 89–112.
- Hill, K. L. (2009) Wind forced low frequency variability in the East Australian Current, Ph.D. thesis, Univ. of Tasmania, Hobart, Tasmania, Australia.
- Hill, K. L., S. R. Rintoul, R. Coleman, and K. Ridgway (2008), Wind forced low frequency variability of the East Australian Current, *Geophys. Res. Lett.*, *35*, L08602, doi:10.1029/2007GL032912.
- Koehl, A., and D. Stammer (2007), Decadal sea level changes in the 50-year GECCO ocean synthesis, *Tech. Rep. 44*, Inst. für Meereskd. Zent. für Meeresch. und Klimaforsch., Univ. Hamburg, Hamburg, Germany.
- Last, P. R., W. T. White, D. C. Gledhill, A. J. Hobday, R. Brown, G. J. Edgar, and G. Peel (2010), Long-term shifts in abundance and distribution of a temperate fish fauna: A response to climate change and fishing practices, *Global Ecol. Biogeogr.*, *20*, 58–72, doi:10.1111/j.1466-8238.2010.00575.x.
- Ling, S. (2008), Range expansion of a habitat-modifying species leads to loss of taxonomic diversity: A new and impoverished reef state, *Oecologia*, *156*(4), 883–894.
- Ling, S., C. Johnson, S. Frusher, and C. King (2008), Reproductive potential of a marine ecosystem engineer at the edge of a newly expanded range, *Global Change Biol.*, *14*, 907–915.
- Lyne, V., R. Thresher, and S. Rintoul (2005), Regional impacts of climate change and variability in South East Australia, workshop report, Commonw. Sci. and Ind. Res. Organ., Clayton, Victoria, Australia.
- Mo, K. C. (2000), Relationships between low-frequency variability in the Southern Hemisphere and sea surface temperature anomalies, *J. Clim.*, *13*, 3599–3610.
- Mulhearn, P. (1987), The Tasman Front—A study using satellite infrared imagery, *J. Phys. Oceanogr.*, *17*, 1148–1155.
- Munk, W. H. (1950), On the wind-driven ocean circulation, *J. Meteorol.*, *7*(2), 79–93.
- Qiu, B., and S. Chen (2006), Decadal variability in the large-scale sea surface height field of the South Pacific Ocean: Observations and Causes, *J. Phys. Oceanogr.*, *36*, 1751–1762.

- Qu, T., and E. J. Lindstrom (2002), A climatological interpretation of the circulation in the western South Pacific, *J. Phys. Oceanogr.*, *32*, 2492–2508.
- Rabe, B., F. Schott, and A. Koehl (2008), Mean circulation variability of the tropical Atlantic during 1952–2001 in the GECCO assimilation fields, *J. Phys. Oceanogr.*, *38*, 117–1192.
- Ridgway, K., R. Coleman, R. Bailey, and P. Sutton (2008), Decadal variability of East Australian Current transport inferred from repeat high-density XBT transects, a CTD survey and satellite altimetry, *J. Geophys. Res.*, *113*, C08039, doi:10.1029/2007JC004664.
- Ridgway, K. R. (2007), Long-term trend and decadal variability of the southward penetration of the East Australia Current, *Geophys. Res. Lett.*, *34*, L13613, doi:10.1029/2007GL030393.
- Ridgway, K. R., and J. R. Dunn (2003), Mesoscale structure of the East Australian Current system and its relationship with topography, *Prog. Oceanogr.*, *56*, 189–222.
- Ridgway, K. R., and J. S. Godfrey (1994), Mass and heat budgets in the East Australian Current: A direct approach, *J. Geophys. Res.*, *99*, 3231–3248.
- Roemmich, D., J. Gilson, J. Willis, P. Sutton, and K. Ridgway (2005), Closing the time-varying mass and heat budgets for large ocean areas: The Tasman Box, *J. Clim.*, *18*, 2330–2343.
- Roemmich, D., J. Gilson, R. Davies, P. Sutton, S. Wijffels, and S. Riser (2007), Decadal spin up of the deep subtropical gyre in the South Pacific, *J. Phys. Oceanogr.*, *37*, 162–173.
- Sasaki, Y., S. Minobe, T. Kagimoto, M. Nonaka, and H. Sasaki (2008), Decadal sea level variability in the South Pacific in a global eddy resolving model, *J. Phys. Oceanogr.*, *38*, 1731–1747.
- Schiller, A., P. Oke, G. Brassington, M. Entel, R. Fiedler, D. Griffin, and J. Mansbridge (2008), Eddy resolving ocean circulation in the Asian-Australian region from an ocean reanalysis effort, *Prog. Oceanogr.*, *76*, 309–316.
- Sutton, P., M. Bowen, and D. Roemmich (2005), Decadal temperature changes in the Tasman Sea, *N. Z. J. Mar. Freshwater Res.*, *39*, 1321–1329.
-
- K. L. Hill, Integrated Marine Observing System, University of Tasmania, Private Bag 110, Hobart, Tas 7001, Australia. (katy.hill@imos.org.au)
- P. R. Oke, K. R. Ridgway, and S. R. Rintoul, Centre for Australian Weather and Climate Research, CSIRO/Bureau of Meteorology, GPO Box 1538, Hobart, Tas 7001, Australia. (peter.oke@csiro.au; ken.ridgway@csiro.au; steve.rintoul@csiro.au)